"Solidification and Deposition of Molten Metal Droplets", M. Chu and E. Lavernia eds., 1998 Annual Meeting, San Antonio, TX, Feb. 15-19, 1998, TMS, Warrendale, PA. pp. 509-520.

SIMULATION OF THERMAL DISTORTION OF A STEEL DROPLET SOLIDIFYING ON A COPPER CHILL

B. G. Thomas and J. T. Parkman

Department of Mechanical and Industrial Engineering
University of Illinois at Urbana-Champaign
1206 West Green Street
Urbana, IL 61801

Abstract

A finite-element model has been developed to predict the evolution of temperature, stress, and shape of 10-mm diameter molten steel droplets solidifying against a water-cooled copper chill plate. The elastic-viscoplastic stress model accounts for thermal linear expansion / contraction behavior, creep, and phase transformations that vary with carbon content. Thermal contraction causes the quenched surface of the impinged droplet to bend away from the chill plate. This creates interfacial resistance that greatly lowers heat transfer. The droplet shape is predicted to evolve almost entirely during the first 0.1 second, when a thin solid skin first forms and becomes strong enough to contract. The final shape of the droplet interface predicted by the model agrees both qualitatively and quantitatively with previous measurements reported by Dong and coworkers. The most deformation, as indicated by the final curvature of solidified droplets, is found in high purity iron (0.003%C) and in peritectic steels (0.12%C). This deformation can be reduced by lowering heat transfer coefficient and avoiding sudden large drops in h. Large drops in heat transfer coefficient also cause reheating of the droplet surface, despite the neglect of nonequilibrium undercooling effects in the model. It is important to minimize surface roughness during initial solidification in order to avoid non-uniform solidification, which is responsible for many casting defects.

Introduction

When molten metal impacts a chilled surface, it suddenly experiences many complex phenomena including rapid cooling, solidification, and thermal distortion. These phenomena control the heat transfer, microstructure, segregation, stresses, and deformation which determine the quality of the cast product. This behavior is critical to many different metals solidification processes besides those involving metal droplets. For example, most of the surface defects in continuous cast steel initiate during the early stages of solidification at the meniscus in the mold. These include surface depressions, longitudinal and transverse surface cracks.

It is well-known that heat transfer during initial solidification is controlled by the contact resistance at the interface between the solidifying metal and the chill. This is affected greatly by the size of the gap, which is controlled by the shape of the solidifying metal surface. Although many previous experimental and heat transfer modeling studies have been done, very little previous attention has been given to predicting thermal distortion during initial solidification. As the solidifying droplet cools and distorts, it may lift away slightly from the substrate, creating gap(s) which greatly lower the heat transfer. This may be sensitive to small changes in composition. The present work is a preliminary attempt to model the evolution of the bottom surface shape of a solidifying steel droplet, in order to better understand these phenomena.

Previous Work

A few recent experimental studies have investigated phenomena during initial solidification, including measurement of the final surface shape. Dong and coworkers [1] melted and levitated 4-8 g droplets of steel and then dropped them 35 mm onto a #1500 Emery-paper-polished and water-cooled copper chill plate, as pictured in Fig. 1. The final shape of the bottom surface of the droplets was measured for different grades and droplet sizes. For small (4-g 10 mm diameter) droplets, the bottom shape could be fit with a parabola, so the curvature was characterized with a single fitting parameter, N_d:

$$\text{gap} = N_d\, y^2 \qquad (1)$$

It was further proposed that N_d could be estimated by one half of the maximum temperature gradient multiplied by the average thermal expansion coefficient. [1] This curvature varied with carbon content, as sketched in Fig. 2. For most droplets, the bottom surface bent away from the chill with a positive N_d curvature and gaps of 100-250 μm. Negative curvatures were observed for carbon contents between 0.6 and 2.5%. Larger droplets had a more complex bottom shape with a depression in the center.

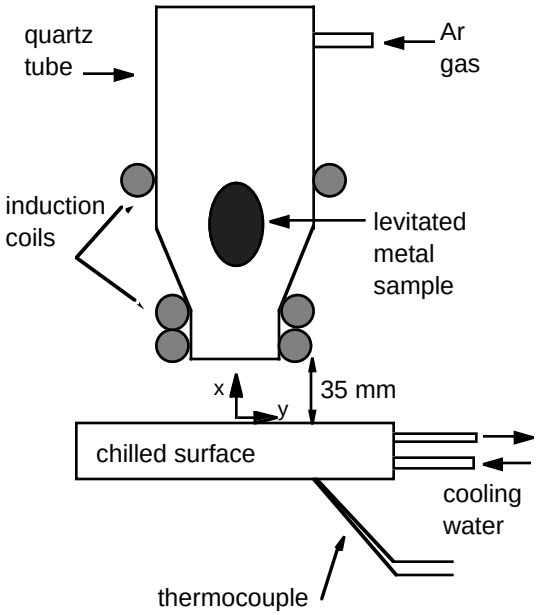

Fig. 1 - Schematic of droplet-quenching apparatus of Dong [1]

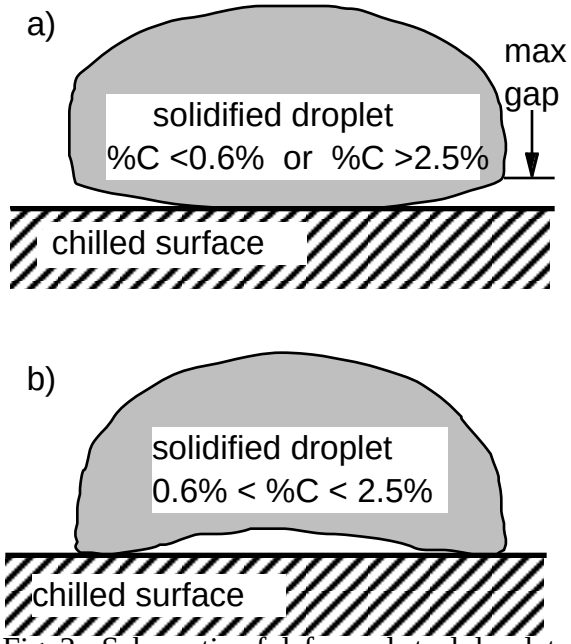

Fig. 2 - Schematic of deformed steel droplets

Todoroki and Cramb [2] solidified stainless steel on a water-cooled copper plate and measured temperatures both in the copper and at the steel interface. Although their droplets were about the same size (3.5 g), the liquid was ejected under 2 atm pressure and more spreading was observed. The heat transfer coefficient was determined to rise quickly (during the first 0.01s) to a maximum of 4 to >12 kW/m^{2}K, and then usually fall to <2 to 5 kW/m^{2}K over 0.5s. The bottom shapes in this work were wavy with mean amplitude (roughness) of 20 - 40 μm. Increasing superheat greatly increases the maximum heat transfer coefficient [2,3] and decreases the final roughness. [2]

Many researchers have observed undercooling of the bottom surface below the equilibrium liquidus temperature, by as much as 300 ˚C, [2,4] followed after about 0.01s by reheating of 50˚C [2] to over 100 ˚C. [4] The undercooling has solutal, curvature, thermal, and kinetic components [4], and is due mainly to delayed nucleation, while the subsequent thermal recalescence is due to sudden latent heat evolution. Others have observed relatively little undercooling or recalescence. [3]

Many researchers have noted the important effect of steel carbon content on the surface roughness of continuously cast steel. Surface roughness, as indicated by the depth of depressions and oscillation marks, is greatest for "peritectic" steel with about 0.1%C. [5-8] Ultra low carbon steel has high roughness also. [8] Higher surface roughness is detrimental because it lowers heat transfer and makes it less uniform. This leads to non-uniform solidification [7] and a greater tendency for cracks and other quality problems in these grades.

It is clear that a better understanding of how surface shape evolves during solidification is critical for improving commercial solidification processes.

Model description

A transient, thermal-elastic-viscoplastic finite-element model, CON2D [9,10] has been developed to follow the thermal and mechanical behavior of a solidifying steel shell. It is applied in this work to simulate stress, strain and distortion in a 2-D section through a 4 gram solidifying droplet, to match conditions of Dong's experiment, [1] pictured in Figures 1 and 2. Due to symmetry, only half of the droplet is simulated.

The model domain, pictured in Fig. 3, is 5 x 6 mm with a graded mesh of 30 x 90 nodes, with an element thickness of 0.041 mm at the metal / substrate interface. The nodes were connected into 2400 3-node triangular elements for the heat transfer analysis. For the stress analysis, 6-node triangular isoparametric elements are used, by connecting sets of four 3-node triangles together. For simplicity, the model in this preliminary work neglects the nonequilibrium phenomena of undercooling and segregation and assumes isotropic properties.

Heat Flow Model: The heat flow model solves the 2-D transient conduction equation, using a fixed Lagrangian grid of 3-node triangles. Latent heat is evolved linearly between the equilibrium liquidus and solidus temperatures which, for standard conditions, are 1535.76 and 1534.63 ˚C (0.003%C steel). Interfacial heat flux is characterized with a uniform heat transfer coefficient between the bottom surface of the droplet and the chill plate, h, that varies with time. For standard conditions, h drops from 20 to 5 kW/m^{2}K at 0.035s, which is an idealization of typical measured behavior. The copper chill is not modeled, as both measurements [2] and calculations show it always stays below 200 ˚C. Heat losses from the side and top of the droplet are ignored.

Stress Model: Starting with stress-free liquid at the meniscus, the stress model calculates the evolution of stresses, strains, and displacements, by interpolating the thermal loads onto a fixed-grid mesh of 6-node triangles. [9] The elastic strain rate vector, $\{\dot{\varepsilon}_e\}$, is related to the total strain rate vector, $\{\dot{\varepsilon}\}$, via:

$$\{\dot{\varepsilon}_e\} = \{\dot{\varepsilon}\} - \{\dot{\varepsilon}_T\} - \{\dot{\varepsilon}_{in}\} - \{\dot{\varepsilon}_f\} \qquad (2)$$

where $\{\dot{\varepsilon}_T\}$ is the thermal strain rate, $\{\dot{\varepsilon}_{in}\}$ is the inelastic strain rate in the solid, and $\{\dot{\varepsilon}_f\}$ is the pseudo-strain rate accounting for flow of the liquid. The out-of-plane z-stress is characterized by the state of generalized plane strain. This allows the 2-D simulations to reasonably estimate the complete 3-D stress state, if bending in the z direction is small.

Ferrostatic pressure is applied from 0.01s onwards, to account for the 6 mm head of liquid steel on the solidification front. The centerline surface node is pinned to prevent rigid body motion and y displacement is set to zero for other nodes on the x-axis symmetry plane. Friction between the mold and solidifying shell is assumed to be negligible.

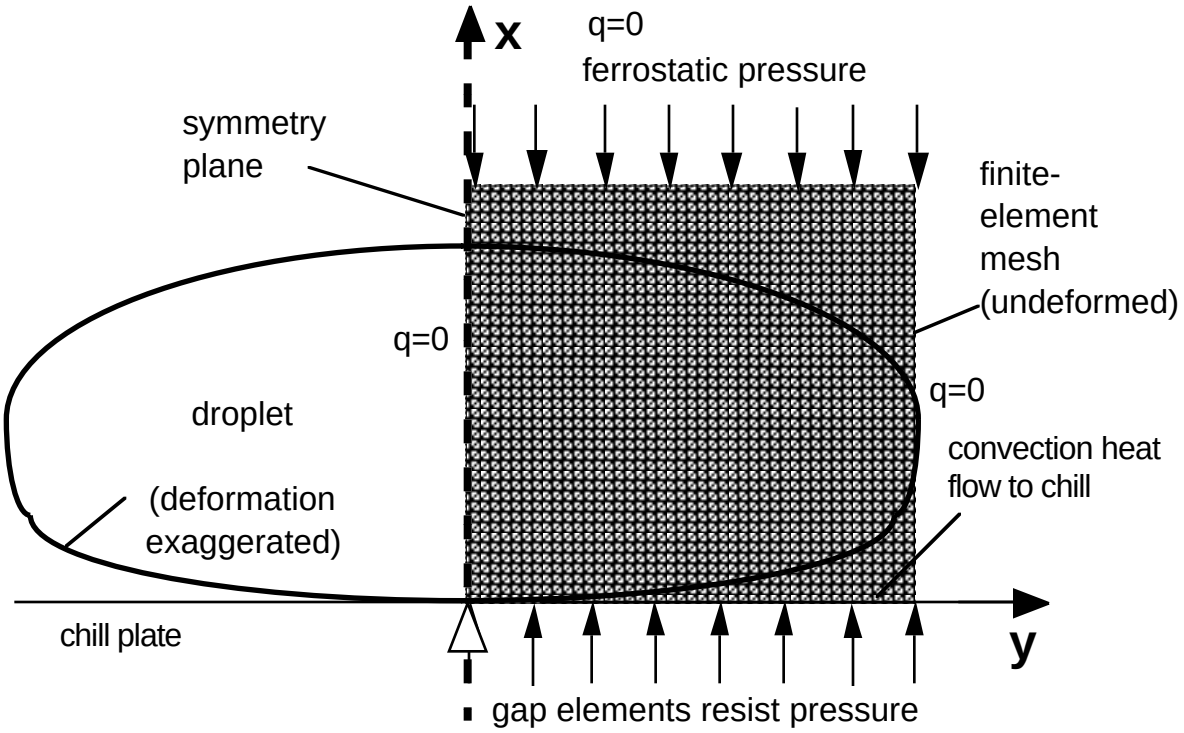

Fig. 3 - Model Domain and boundary conditions

Elastic Strain: Stress is caused solely by elastic strain. The elastic modulus decreases with increasing temperature, based on data measured by Mizukami et al [11].

Thermal Strain: Thermal strains arise from volume changes caused by both temperature differences and phase changes (including both solidification and solid state transformations). They are calculated from the temperatures determined in the heat transfer analysis, {T}, and the state function TLE, or **t**hermal **l**inear **e**xpansion of the material. All strains, including those from phase transformations are assumed to be isotropic. For example, $\{\varepsilon_T\} = (TLE(T) - TLE(T_o)) \{1,1,0,1\}^T$. This neglects anisotropic effects, which may arise during columnar dendrite solidification. TLE is found from the temperature-dependent mass density. In mixed phase regions, TLE is found from a weighted average using the TLE curves for each of the individual phases present, based on their volume fractions. During steel solidification and cooling, liquid (l), delta ferrite (δ), austenite (γ), alpha ferrite (α) and iron carbide (Fe_3C) may be present:

$$TLE = (\%L)\, TLE_L + (\%\delta)\, TLE_\delta + (\%\gamma)\, TLE_\gamma + (\%\alpha)\, TLE_\alpha + (\%Fe_3C)\, TLE_{Fe3C} \quad (3)$$

The TLE functions and phase fractions are calculated as a function of temperature and carbon content. The model adopts TLE functions for plain carbon steel, (Figure 3) based on solid phase density data by Harste [12] and liquid density data from Jimbo and Cramb. [13] Phase fractions are estimated using the equilibrium Fe-C phase diagram, so nonequilibrium phases due to slow nucleation kinetics are neglected.

Figure 4 shows the thermal linear expansion of steel assumed in the model as a function of carbon content. Thermal strain, and the associated stress and deformation, depend only on relative changes between points on a given curve. Nevertheless, reference temperatures were chosen such that TLE is 2.5% at the equilibrium solidus temperature for each curve, so that solid phase contraction can be compared between grades. Note that liquid shrinkage during solidification is much larger than solid shrinkage. This figure shows that the total shrinkage from solidus to 1300 ˚C increases with decreasing carbon content. This shrinkage is greatest for the steels which experience a transformation from delta to austenite (See 0.1% and 0.003% C).

Inelastic strain: Inelastic strain includes strain in the solid arising from both creep and plastic yielding. Constitutive behavior for solidifying plain-carbon steel was simulated using the rate-dependent, elastic-viscoplastic model III of Kozlowski. [14] This model was developed to match tensile test measurements of Wray [15] and creep data of Suzuki [16] over a range of strain rates, temperatures, and carbon contents to simulate austenite under continuous casting conditions. These equations were extended to model the enhanced creep rate in delta ferrite, and compare reasonably with tensile-test data from Wray, [17] as shown in Figure 4.

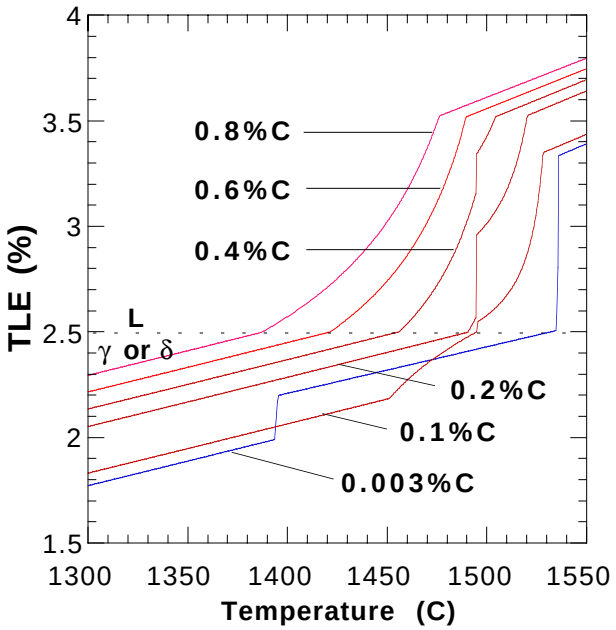

Fig. 4 - Thermal linear expansion of steel for different %C (data from Harste, [12] and Jimbo [13])

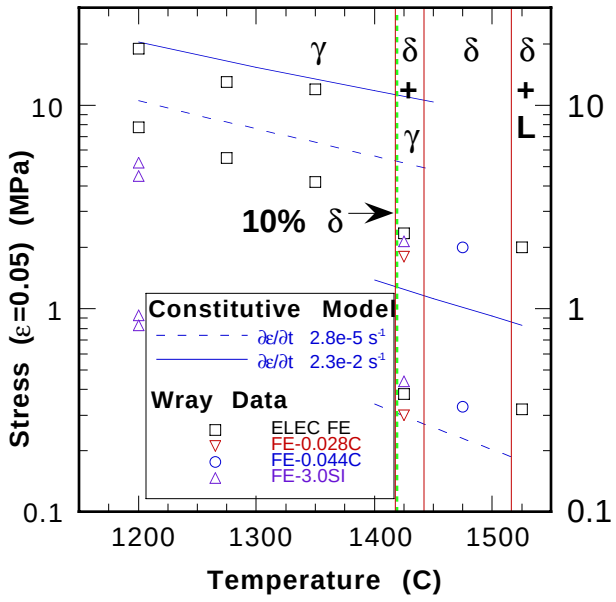

Fig. 5 - Comparison of predicted and measured stress, [17] showing δ-ferrite is weaker than γ

Flow Strain: The model assumes that when liquid is present, fluid flow will occur to exactly match the shrinkage. Elements are treated as liquid when any node in the element is above the specified coherency temperature (set to solidus). Liquid elements are set to have no elastic strain, and consequently develop no stress. The difference between the total strain and thermal strain in liquid elements is assumed to be made up by a "flow strain". This flow strain is needed for future work to model segregation and crack formation, but has no effect in this work.

Solution Details: This model features an efficient algorithm to integrate the highly non-linear constitutive equations. A new two-level solution algorithm has been implemented, which alternates between solutions at the local node point and the global system equations. [6] To minimize numerical errors, a very fine, graded mesh was required, including 90 nodes per row across the 6 mm thick shell. The time step size varies from 0.0001s initially to 0.005s at 1s to 0.01s beyond 2s. Each 20s simulation needed about 30 hours on an IBM RS6000-370.

Model Validation: The model has been validated with measurements from breakout shells in continuous slab casters, and analytical solutions, described in detail elsewhere. [9, 10] Figures 7 and 8 show model predictions of temperature and stress generation at 10s during 1-D solidification of an

infinite planar slab into an semi-infinite domain. The predictions compare almost exactly with the analytical solution from Boley and Weiner. [18] At earlier times, the results fluctuate or "wiggle" due to discretization errors, but still match reasonably well.

This example problem assumes instant quenching of the slab surface to 1300 ˚C from the liquid (initially at the unique solidification temperature of 1468 ˚C). Yield stress, σ_y, was assumed to increase with lower temperature, according to σ_y (MPa) = 0.119 [1468 - T(˚C)]. The elastic-perfectly-plastic constitutive model was approximated with a penalty function approach. [2] Other thermal and mechanical properties are: 7400 kg/m^3 density, 700 J/kgK specific heat; 33 W/m-K thermal conductivity; 272 kJ/kg latent heat, 0.35 Poison ratio, 0.00002 K^{-1} thermal expansion coefficient, and 40 GPa elastic modulus.

Fig. 8 shows that the slab surface goes into compression in this example. This is because the surface layer solidifies and cools stress free. As each inner layer solidifies, it cools and tries to shrink while the surface temperature remains constant. Because the slab is constrained to remain planar, complementary subsurface tension and surface compression stresses are produced. These stresses are much higher than found in a droplet which is able to deform. The surface compression is a driving force to bend the slab or droplet surface into the shape measured for low carbon steel (Fig. 2 a).

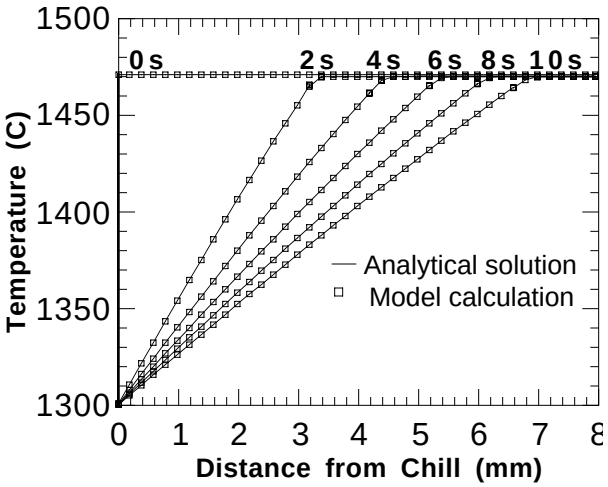

Fig. 6 - Predicted and analytical temperature profiles in slab solidification problem [18]

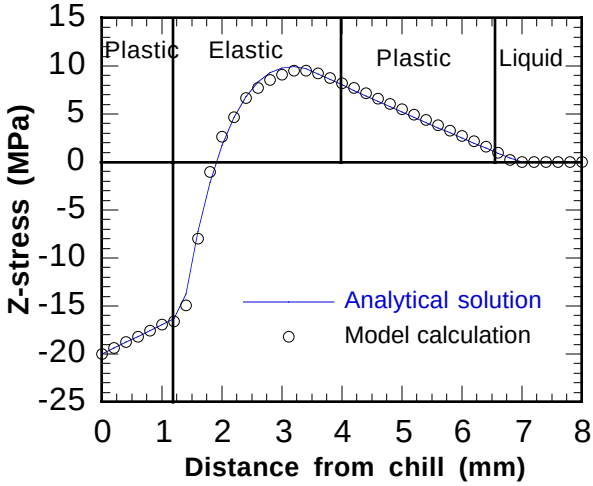

Fig. 7 - Comparison of predicted and analytical [18] stress through slab thickness (at 10s).

Results

Typical simulation results are presented in Figs. 8-10, for .003%C steel. Temperature profiles through the droplet at short times (Fig. 8a) show that the initial temperature gradient is very steep near the surface, owing to the high initial heat transfer coefficient of 20 kW/m^{2}K. Then, the sudden drop in h at 0.035s causes the surface gradient to decrease, so heat from inside the droplet is conducted to the surface faster than it can be removed. This makes the surface reheat by 115 ˚C. This is comparable to the measured surface reheating, but should not be mistaken for classic recalescence due to undercooling, which is not possible in this model.

Another sharp drop in temperature gradient accompanies complete solidification of the droplet at 4.8s. This drop would be larger if cooling from the top surface were not zero. Temperature gradients drop gradually after this until ambient temperature is reached throughout.

The distortion results in Fig. 9 show a close correspondence with the temperature gradient results. For the first 0.035s, the droplet contacts the chill surface closely, because any solid that forms is too thin, hot, and weak to support even the tiny ferrostatic pressure generated by the mass of the droplet. When a thin layer of solid reaches a critical thickness, it is able to support

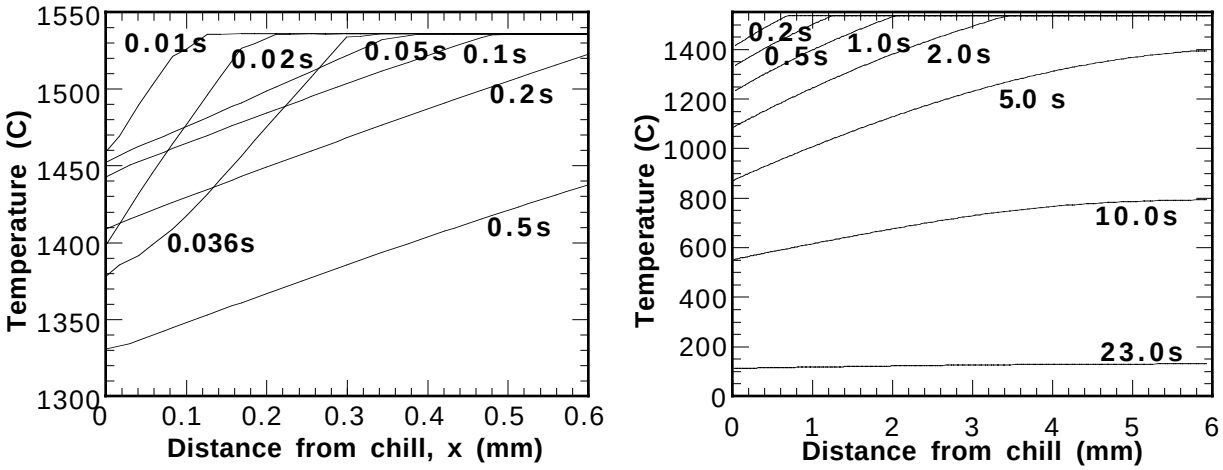

Fig. 8 - Evolution of temperature profiles through droplet
a) Short times b) Long times

this pressure, and further cooling relaxation of the temperature gradients causes it to bend away from the chill plate. At that instant, a sudden drop in convective heat transfer is imposed. This rapidly accelerates the bending, leading to a maximum gap at the droplet edge of over 170 μm by 0.05s, as shown in Fig. 9a. This increase in contraction accompanying the drop in heat transfer is a well-known instability, as it encourages further drops in h and further contraction. The surface profile remains relatively constant until the droplet completely solidifies. The associated drop in temperature at the time of final solidification produces a further bending to 200 μm. Further cooling produces only minor changes in the gap. Thus, the final curved shape of droplet surface is determined almost completely during the initial contraction event during the first 0.1s of solidification.

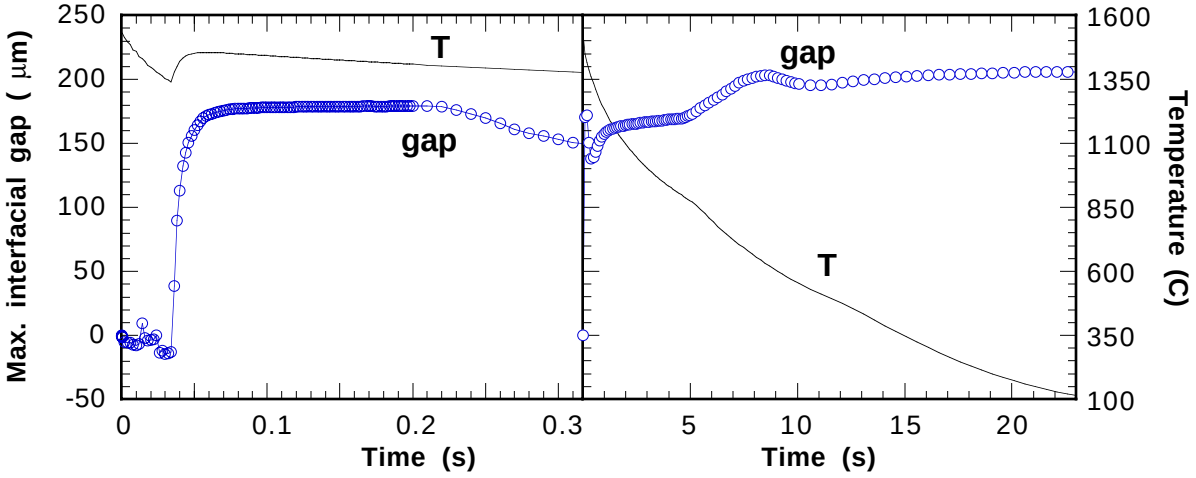

Fig. 9 Evolution of temperature and maximum interfacial gap (edge of droplet in Fig. 2)
a) - Short times b) Long times

Figure 10 shows the calculated shell growth history. The start of contraction and drop in heat transfer coefficient occurs when the shell is < 0.3 mm thick. For the equilibrium conditions assumed, the solidification rate drops from roughly 10 mm/s initially to 2 mm/s at 1s to less than 1 mm/s when the droplet solidifies at 4.8s. This rate is almost three orders of magnitude slower than the growth rate predicted with 100 ˚C undercooling. [4] Thus, if any undercooling occurs, the solidification front will quickly grow to the thickness given in Fig. 10, as soon as nucleation finally starts. The drop in solidification rate which follows this rapid initial spurt is likely responsible for the sharp change in microstructure commonly seen near the surface of rapidly

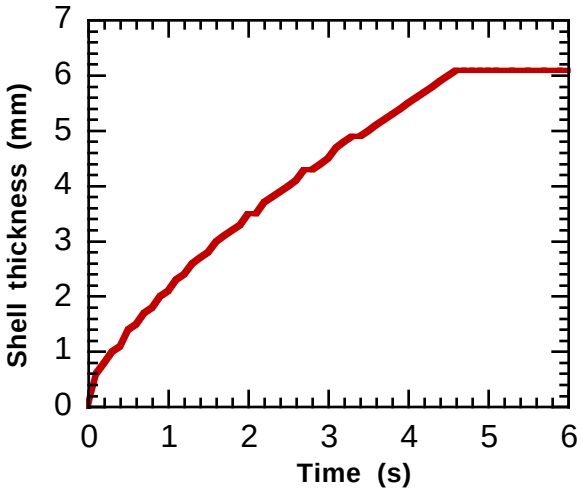

Fig. 10 - Calculated shell growth history

solidified steel.

Figure 11 shows the predicted y stress profiles at several important times. The initial stress profile (0.5s) is qualitatively similar to that in Fig. 7, with compression along the droplet surface and tension towards the interior. The magnitudes are slightly lower, however, owing to the stress relief of bending. The temperature gradients, deformation, and stresses do not change significantly for the next 5s. After complete solidification of the droplet, however, temperature gradients within the droplet relax, which sets up significant tensile stress in the droplet interior and balancing compression in both exterior layers.

Figure 12 shows the calculated curved shape of the bottom surface of the droplet, at 23s, when the final temperature was just over 100 ˚C. The best parabolic curve fit through the points produced N_d (Equation 1) of 9.05 m^{-1}. The match is consistent with both the measurements of Dong and coworkers [1], and their simple mechanical bending model.

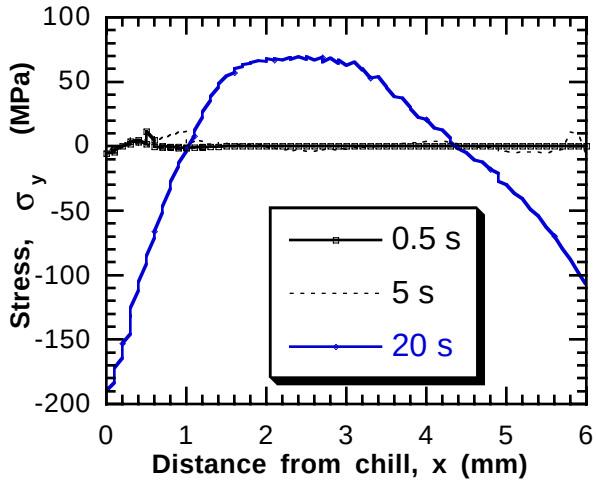

Fig. 11 - Evolution of transverse stress profiles through droplet

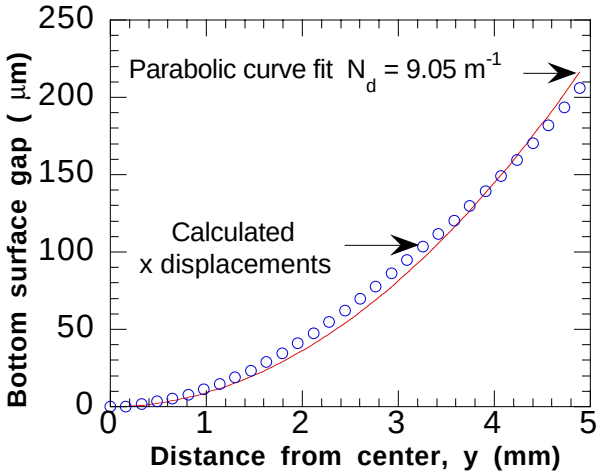

Fig. 12 - Final shape of droplet surface (calculations and fitted parabola)

Effect of heat transfer coefficient

The heat transfer coefficient during initial solidification can vary greatly. Its effect on deformation is explored parametrically with the results in Figs. 13 -15. Even with a constant heat transfer coefficient, Fig. 13 shows that the droplet surface breaks away from the chill and adopts the curved shape shown in Fig. 2a. This simulation was performed without ferrostatic pressure, which allows the shell to bend initially towards the chill (as in Fig. 2b). The brief period of initially reversed bending is prevented by pressure in all other runs.

Shell bending generally increases in proportion to the drop in temperature gradient. Fig. 14 shows that lowering the final heat transfer coefficient slightly increases the bending at early times. This is because there is a greater drop in temperature gradient while the shell is still thin. The effect on increasing final curvature is smaller.

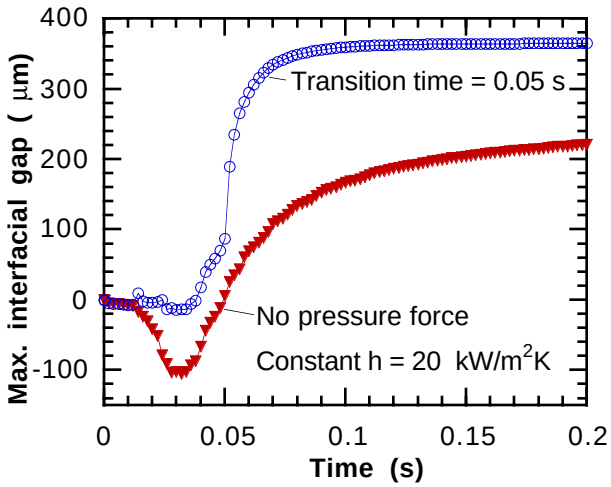

Fig. 13 Effect of pressure and transition time on gap history (0.003%C)

A sudden drop in convection coefficient causes an immediate increase in bending, as previously discussed. If this sudden drop occurs earlier during solidification, the shell will be thinner and the change in temperature gradient will be larger. Consequently, more bending will occur, producing a larger final curvature. This trend of shorter transition times leading to more bending can be observed in the results in Fig. 15. Specifically, for 0.23 %C steel, decreasing the transition time from 0.30 to 0.05 s causes N_d to increase from 7.1 to 8.9 m^{-1}. For 0.16 %C steel, decreasing the transition time from 0.15 to 0.04 s makes N_d increase from 8.0 to 9.6 m^{-1}. This finding suggests that bending curvature (and related problems from the corresponding uneven surface) can be reduced by avoiding sudden huge decreases in heat transfer coefficient. This is best done by reducing the maximum heat transfer coefficient.

Fig. 13 includes a run that shows the large increase in bending that occurs when h is suddenly decreased at 0.05s for 0.003%C steel. By delaying the transition time to 0.05s, the surface temperature was allowed to fall below 1300 ˚C, forming a significant layer of austenite while the shell was still flat. When the surface reheated to 1430˚C, this cold surface layer transformed back to delta ferrite, producing an expansion that generated further bending. The final curvature of 14 greatly exceeds that for the shorter transition time of 0.035s. Thus, longer transition times may not always lead to less bending, if there are phase transformations.

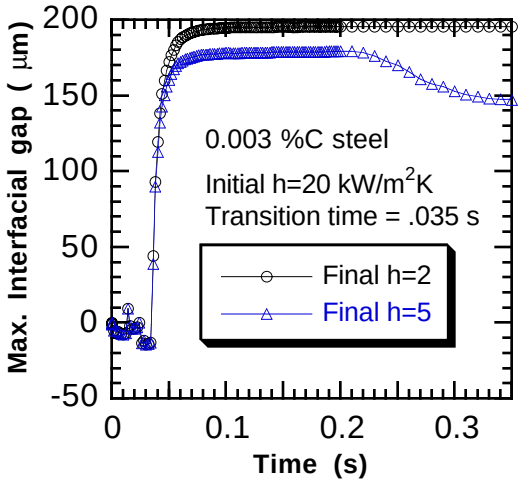

Fig. 14 - Effect of final heat transfer coefficient on shrinkage

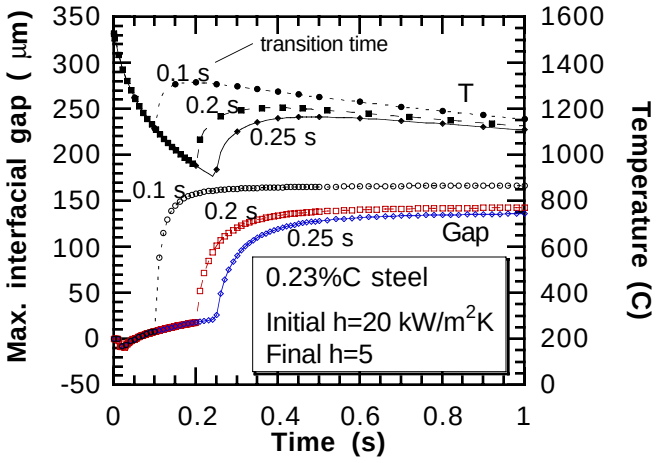

Fig. 15 - Effect of transition time on temperature and displacement histories.

Effect of Carbon Content:

Carbon content of the steel has several important effects on the behavior just presented. This work considers only its effects on creep rate and volume changes, associated with the phase transformations. Five different carbon contents were simulated, for conditions given in Table I. In each case, the heat transfer coefficient was assumed to drop from 20 to 5 kW/m^{2}K at a transition time chosen, through trial and error, to match the time when the solid first lost contact and pulled away from the mold. Finally, the curvature N_d, was found at about 22s when temperature had fallen to about 100 ˚C and compared with measured values in Fig. 15. [1]

Table I Simulation Conditions and Results for Varying Carbon Contents

Run	Superheat	Liquidus	Solidus	Transition time	Nd
0.003%C	0.24 ˚C	1535.76	1534.63	.035 s	9.1
0.05% C	4.0	1532.06	1513.22	.025 s	5.6
0.12 % C	9.5	1526.54	1495	.015 s	12.0
0.16 %C	12.6	1523.38	1495	.040 s	9.6
0.23 %C	18.1	1517.87	1485.34	.050 s	8.9

At the droplet surface, the inelastic and elastic strains are relatively small, so the total strain roughly matches the thermal strain accumulated in the solid. The effect of composition on deformation is thus expected to relate to thermal strain, given in Fig. 5. The lower carbon steels thus have the largest curvatures, other phenomena being equal.

The results in Fig. 16 match the measured behavior for low carbon steel droplets very well. However, the model consistently overpredicts the distortion and the negative curvatures of higher carbon steels (Fig. 2b) could not be sustained. The agreement may be fortuitous, considering the tremendous oversimplifications in the model. Several observations are noteworthy, however.

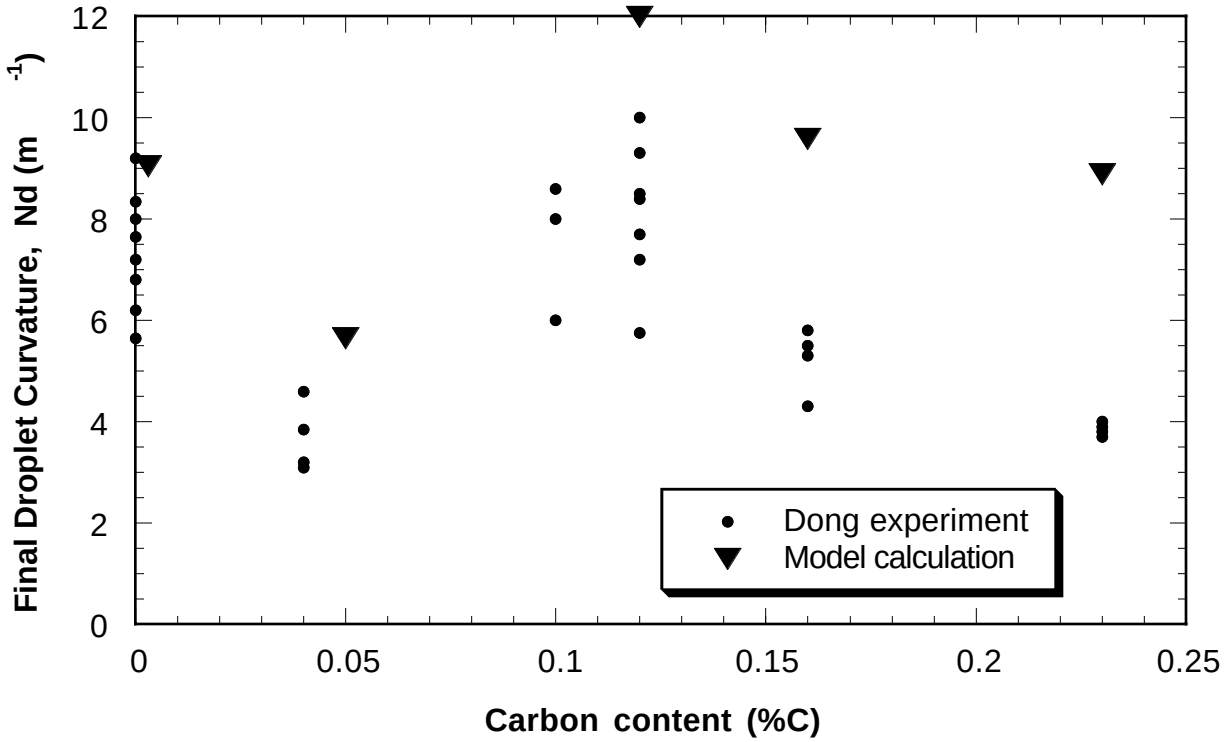

Fig. 16 - Comparison of predicted and measured droplet distortion for different steel grades (Standard conditions in Table I)

The 0.12%C steel is predicted to have the most curvature, in part because it pulls away from the mold earlier than the other grades, so was modeled with a shorter transition time. This is due to its experiencing the large delta to austenite thermal contraction at a higher temperature than any other grade. The shrinkage occurs closer to the solidification front, so strengthens the shell faster. [19] This enables the 0.12% steel shell to overcome the ferrostatic pressure sooner than the other steels. By breaking away from the chill sooner, this steel experiences the drop in heat transfer sooner. The corresponding drop in thermal gradient is much greater, so the final curvature is a maximum. Note that the very low carbon steel (0.003%C) behaves in a similar manner.

In contrast, the 0.23%C steel pulls away from the chill very slowly, as shown in Fig. 15. Without a decrease in h, the gap remains very small, even after 0.25s. This long time allows temperature gradients to drop before the bending gets started, so the final curvature is less. The 0.05%C steel has

a small curvature despite a reasonably large thermal contraction (Fig. 4) because its transition time is long. Note that higher superheat tends to extend the time required to achieve a given shell thickness, thus extending the transition time. The effect of transition time depends on the solidified thickness at the time of the transition. This thickness depends on many factors, including the initial heat transfer coefficient history, the superheat, and non-equilibrium delays waiting for nucleation.

These results suggest that a high cooling rate is doubly detrimental to shell bending in peritectic steels. In addition to the steep temperature gradients produced, cooling rates of more than 5000 C/s are reported to induce direct transformation to metastable cellular austenite. [4] When the resulting surface austenite layer reheats a few milliseconds later, it transforms to delta and expands. Combined with a rigid subsurface layer, the result would be a tremendous increase in bending, relative to other grades.

Discussion

This work is a crude first attempt to quantitatively predict the shape of solidified surfaces. The encouraging results of this work suggest that the characteristic curved bottom shape observed in Fig. 2a is consistent (both qualitatively and quantitatively) with thermal stress generation in a solidifying droplet in the absence of friction. The wavy final bottom shapes observed after solidification of larger droplets or with higher pressure might be caused by fluid overflowing the initially solidifying region. The liquid surface at the edge of the droplet is subject to very high temperature gradients, so surface tension effects including Marangoni-driven flow and dynamic changes in contact angle could greatly affect droplet spreading when liquid first contacts the chill. The direction of these forces is very sensitive to small composition changes, such as low S levels in steel. These phenomena together may cause the solidifying surface of a large volume of metal to behave mechanically like a series of barely connected droplets.

This mechanism is likely complicated by the distribution or shortage of nucleation sites, intermittent surface contact and sticking adhesion, and mechanical bending associated with the nonuniform heat transfer. Prediction of the critically-important convection heat transfer coefficient is a difficult coupled problem that is time and position dependent. In addition to the size of the gap, h depends on the thermal properties of the medium that fills the gap, the condition of the chill surface, and how well the molten metal initially contacts the chilled surface, which may depend on the surface tension (which may in turn vary with superheat and composition). The anisotropic properties of columnar dendrites will produce different mechanical behavior in the x and y directions. Finally, quantitative prediction of surface shape also requires proper consideration of nonequilibrium phase transformation, undercooling, microsegregation, and other effects such as gas evolution and entrapment. Clearly, much work remains to be done before the shape of solidified surfaces can be predicted with confidence.

Conclusions

A transient finite-element model has been verified with analytical solutions and applied to predict temperature and thermal distortion of a steel droplet solidifying against a chill plate. The findings suggest that:

1) Model predictions of final surface shape of the droplet agree surprisingly well with measurements [1] for several different carbon contents.

2) The observed drop in heat transfer coefficient, and corresponding rise in surface temperature appear to coincide with the formation of a critical thickness of solidified metal with sufficient strength to bend away from the chilled surface.

3) Surface shape evolves almost completely within the first 0.03 - 0.2 second of the droplet impacting the chill plate. The shorter times apply to lower carbon contents, which produce a strong thin shell more quickly.

4) The increase in surface temperature observed in experiments might not be due entirely to recalescence related to delayed nucleation and latent heat evolution. Surface reheating is predicted even with this equilibrium solidification model, when the surface heat transfer coefficient drops suddenly.

5) Creep and bending relax almost all of the stresses until the droplet is completely solid.

6) A sudden decrease in h causes generally causes more bending when it occurs earlier, unless phase transformations reverse.

7) A very fine mesh and time step are needed to obtain grid-independent model predictions.

The surface roughness predicted here is likely responsible for non-uniform heat transfer and accompanying defects. Further work is needed to investigate this important behavior.

Acknowledgments

The authors wish to thank the Continuous Casting Consortium at UIUC, including AK Steel, (Middletown, OH), Allegheny Ludlum, (Brackenridge, PA), Armco Inc. (Middletown, OH), Inland Steel Corp. (East Chicago, IN), LTV (Cleveland, OH), and Stollberg, Inc., (Niagara Falls, NY) for their continued support of our research and the National Center for Supercomputing Applications (NCSA) at the UIUC for computing time.

References

1. S. Dong, E. Niyama and K. Anzai, ISIJ Internat., 35 (6) (1995), 730-736.
2. H. Todoroki et. al., (Paper presented at Steelmaking Proceedings, Chicago, IL, 1997, Iron and Steel Society), 80.
3. G.X. Wang and E.F. Matthys, J. Heat Transfer, 118 (Feb.) (1996), 157-163.
4. H. Mizukami et. al., Mat. Sci. & Eng., A173 (1993), 363-366.
5. R.B. Mahapatra, J.K. Brimacombe and I.V. Samarasekera, Metallurgical Transactions B, 22B (December) (1991), 875-888.
6. A.W. Cramb and F.J. Mannion, in Steelmaking Proceedings, 68, (Warrendale, PA: Iron and Steel Society, 1985), 349-359.
7. B.G. Thomas, D. Lui and B. Ho, (Paper presented at Applications of Sensors in Materials Processing, Orlando, FL, 1997, TMS, Warrendale, PA).
8. M. Suzuki et. al., ISIJ Internat., 36 (1996), S171-S174.
9. H. Zhu, "Coupled Thermal-Mechanical Fixed-Grid Finite-Element Model with Application to Initial Solidification" (PhD Thesis, University of Illinois, 1997).
10. A. Moitra, "Thermo-mechanical model of Steel Shell Behavior in Continuous Casting" (Ph.D. Thesis, University of Illinois at Urbana-Champaign, 1993).
11. H. Mizukami, K. Murakami and Y. Miyashita, Tetsu-to-Hagane, 63 (146) (1977), S 652.
12. K. Harste, A. Jablonka and K. Schwerdtfeger, (Paper presented at 4th Int. Conf. on Continuous Casting, Centres de Recherches Metallurgiques and Verein Deutscher Eisenhuttenleute, 1988, Stahl und Eisen, Brussels), 633-644.
13. I. Jimbo and A. Cramb, Metall. Trans. B, 24B (1993), 5-10.
14. P. Kozlowski et. al., Metall. Trans. A, 23A (March) (1992), 903-918.
15. P.J. Wray, Metall. Trans. A, 13A (1) (1982), 125-134.
16. T. Suzuki et. al., Ironmaking Steelmaking, 15 (2) (1988), 90-100.
17. P.J. Wray, Metall. Trans. A, 6A (1976), 1621-1627.
18. J.H. Weiner and B.A. Boley, J. Mech. Phys. Solids, 11 (1963), 145-154.
19. B.G. Thomas and J.T. Parkman, (Paper presented at Thermec 97 Internat. Conf. on Thermomechanical Processing of Steel and Other Materials, Wollongong, Australia, 1997, TMS).